Charge Condensation and Lattice Coupling Drives Stripe Formation in Nickelates

Y. Shen,[1,*] G. Fabbris[1,2] H. Miao[1,3] Y. Cao,[1,4] D. Meyers,[1,5] D. G. Mazzone[1,6] T. Assefa[1] X. M. Chen,[1]
K. Kisslinger,[7] D. Prabhakaran,[8] A. T. Boothroyd,[8] J. M. Tranquada[1] W. Hu,[9] A. M. Barbour,[9] S. B. Wilkins,[9]
C. Mazzoli,[9] I. K. Robinson,[1] and M. P. M. Dean[1,†]

[1]*Condensed Matter Physics and Materials Science Department, Brookhaven National Laboratory, Upton, New York 11973, USA*
[2]*Advanced Photon Source, Argonne National Laboratory, Lemont, Illinois 60439, USA*
[3]*Material Science and Technology Division, Oak Ridge National Laboratory, Oak Ridge, Tennessee 37830, USA*
[4]*Materials Science Division, Argonne National Laboratory, Lemont, Illinois 60439, USA*
[5]*Department of Physics, Oklahoma State University, Stillwater, Oklahoma 74078, USA*
[6]*Laboratory for Neutron Scattering and Imaging, Paul Scherrer Institut, CH-5232 Villigen, Switzerland*
[7]*Center for Functional Nanomaterials, Brookhaven National Laboratory, Upton, New York 11973, USA*
[8]*Department of Physics, University of Oxford, Clarendon Laboratory, Oxford OX1 3PU, United Kingdom*
[9]*National Synchrotron Light Source II, Brookhaven National Laboratory, Upton, New York 11973, USA*

Revealing the predominant driving force behind symmetry breaking in correlated materials is sometimes a formidable task due to the intertwined nature of different degrees of freedom. This is the case for $La_{2-x}Sr_xNiO_{4+\delta}$, in which coupled incommensurate charge and spin stripes form at low temperatures. Here, we use resonant x-ray photon correlation spectroscopy to study the temporal stability and domain memory of the charge and spin stripes in $La_{2-x}Sr_xNiO_{4+\delta}$. Although spin stripes are more spatially correlated, charge stripes maintain a better temporal stability against temperature change. More intriguingly, charge order shows robust domain memory with thermal cycling up to 250 K, far above the ordering temperature. These results demonstrate the pinning of charge stripes to the lattice and that charge condensation is the predominant factor in the formation of stripe orders in nickelates.

Emergent phenomena in strongly correlated materials arise due to multifarious interactions among charge, spin, and lattice degrees of freedom. Such complexity hampers the ability to understand their remarkable states and realize new functionalities [1]. Identifying dominant interaction is, however, challenging, as different interactions act simultaneously and can yield complex ground states with more than one form of order [2]. A representative phenomenon of this type is the electronic stripes that appear in various strongly correlated materials [3–6]. These effects have been considered extensively in cuprate high-temperature superconductors, which host charge and sometimes spin stripe order, typically with a simple factor-of-2 relationship between the charge and spin incommensurabilities [7–9]. Nickelates also host both superconductivity and stripe order [10–12], but no system has yet been shown to simultaneously host both orders. The existence of stripe order in $La_4Ni_3O_8$, which appears rather similar to superconducting $Nd_{1-x}Sr_xNiO_2$ [13–16], does, however, support the likely proximity of stripe order and superconductivity. While static stripe order appears to suppress bulk 3D superconductivity, some researchers have suggested that stripe fluctuations may act to promote superconductivity [17–19]. Therefore, understanding the driving forces behind charge and spin stripe formation and dynamics in strongly

correlated materials has attracted considerable attention and may be crucial to understanding unconventional superconductivity. Stripe formation has been studied in the past through detailed measurements of stripe transition temperatures and correlation lengths [20–28] and associated Landau model analysis [29,30]. The problem has also been addressed via model Hamiltonian analysis that suggested that lattice coupling might be crucial to stabilize stripes [31,32]. The implementation of resonant x-ray photon correlation spectroscopy (XPCS) at modern low-emittance synchrotron sources opens new routes to directly probe stripe formation and dynamics [33–36].

Herein, we report the first resonant XPCS experiment to simultaneously probe charge order (CO), spin order (SO), and lattice coupling in a stripe-ordered material, focusing on the prototypical material $La_{2-x}Sr_xNiO_{4+\delta}$ (LSNO) with $x = 0.225$ and $\delta = 0.07$. Although SO is more correlated and stable at 70 K, CO is more robust in temporal stability against temperature changes, which we attribute to electron-phonon coupling (EPC). This is further supported by our discovery that the CO domains are effectively pinned to the lattice and the corresponding speckle patterns remain highly reproducible with thermal cycling up to 250 K, well above the transition temperature T_{CO}. SO, however, is not directly coupled to the lattice and loses its domain memory

once the sample is warmed across the magnetic transition temperature T_{SO}. These results imply that charge condensation, and its coupling to the lattice and disorder, is the driving force behind stripe ordering.

X-ray measurements were carried out at the Coherent Soft X-Ray (CSX) 23-ID-1 beam line at the National Syncrotron Light Source II with x-ray energy tuned to the Ni L_3 edge [Fig. 1(a)]. The LSNO single crystal was synthesized by the
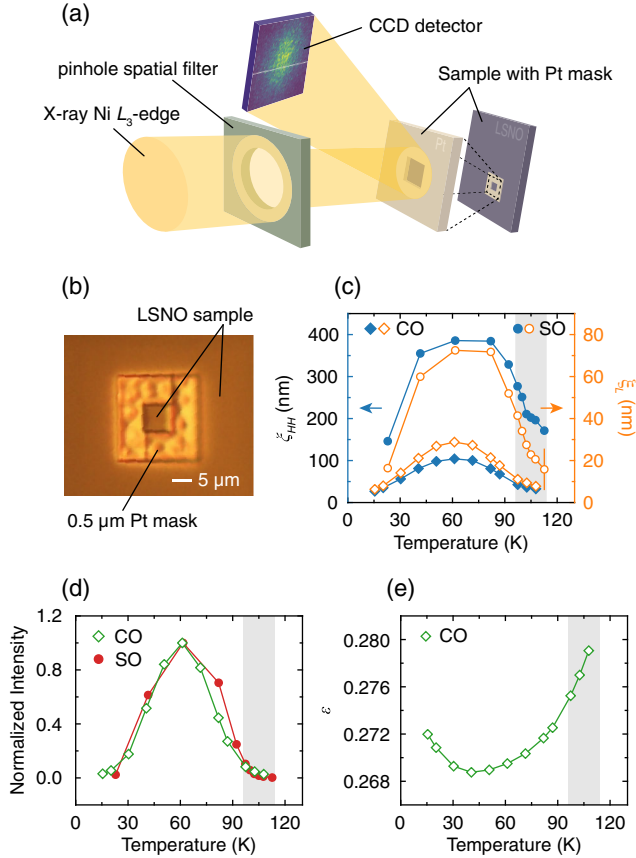

FIG. 1. Experimental configuration and CO and SO superlattice peaks. (a) The instrumental setup for the measurements at CSX. The x-ray beam is set to the Ni L_3-edge energy and tuned in order to maximize the strength of the CO and SO intensity [39]. It then propagates through the pinhole and is scattered by the LSNO sample onto the detector. For the domain memory study, a 0.5-μm-thick Pt mask was deposited on the sample [39]. (b) An optical micrograph of the Pt mask on the (110) surface of a LSNO single crystal. (c) Temperature dependence of the correlation lengths along $[H, H, 0]$ and $[0, 0, L]$ directions. The correlation length is defined as $\xi = d/\text{HWHM}$, where HWHM stands for half width at half maximum in reciprocal lattice units and d is the unit cell size in the appropriate direction [44]. (d) Temperature dependence of the peak heights evaluated from fitting of the CO and SO superlattice peaks, which are normalized according to their values at 60 K. The signals were fitted with a three-dimensional Lorentzian function. (e) Incommensurability defined by the peak position of the CO $\boldsymbol{Q}$ vector as a function of the temperature. The shaded areas indicate the onset temperature range for CO and SO.

floating-zone method with a Sr concentration of $x = 0.225$ [37]. As shown later, the CO incommensurability is $\epsilon \approx 0.27$, larger than x, which is likely related to oxygen doping, since $\delta = 0.07$ [38]. The sample's surface normal was close to the $[H, H, 0]$ direction. Thus, we made (H, H, L) the scattering plane and focused on peaks with $\boldsymbol{Q}_{CO} = (\epsilon, \epsilon, 1)$ and $\boldsymbol{Q}_{SO} = (1/2 - \epsilon/2, 1/2 - \epsilon/2, 0)$ [39]. The reciprocal lattice units (r.l.u.) is defined in terms of $\boldsymbol{Q} = (H, K, L) = (2\pi/a, 2\pi/b, 2\pi/c)$ within the space group I4/mmm and $a = b = 3.84$ Å and $c = 12.65$ Å. For the domain memory measurements, we used a 0.5-μm-thick Pt mask, which had been deposited on the sample in order to reproducibly illuminate the same sample volume independent of possible thermal drifts in the sample position [Fig. 1(b)] [39].

We start by characterizing the superlattice peaks corresponding to CO and SO at different temperatures using standard resonant x-ray diffraction. With decreasing temperature, the peak heights first increase substantially through the transition temperatures along with enhanced correlation lengths for both CO and SO [Figs. 1(c) and 1(d)]. Below $\sim$70 K, the peak heights drop and the spatial correlations are relaxed, consistent with previous reports [26,45,46]. The reason for this is not uniquely determined, but it may be connected to a spin reorientation at lower temperature [27] or the influence of spin exchange interactions [26]. Throughout the temperature range, the correlation lengths along the $[H, H, 0]$ direction are much larger than those along $[0, 0, L]$ and SO possesses a larger correlation length than CO [Fig. 1(c)]. Because of the critical fluctuations and short-range correlations near the phase transitions, the onset temperatures T_{CO} and T_{SO} are not uniquely defined. We estimate them both to occur between 96 and 114 K. Regarding the incommensurability, the intersite Coulomb repulsion tends to stabilize ϵ equal to the hole concentration [47], while the commensurability effect optimizes stripe formation at $x = 1/3$. The actual incommensurability is a compromise of these two factors [23]. With increasing temperature, thermal fluctuations are expected to start to outcompete Coulomb repulsion [45,48,49], driving the incommensurability closer to $1/3$ at higher temperature [Fig. 1(e)].

To elucidate the temporal stabilities of CO and SO, we employ XPCS to study the domain distribution and its fluctuations. In XPCS, the coherent photons scattered by different domains interfere with each other, leading to a complex "speckle" pattern modulated by the usual diffraction line shape [33,34,36,50–52]. Figures 2(a) and 2(b) show the representative speckles of the CO and SO superlattice peaks at 70 K. The shape of the peak envelope is determined by the spatial correlations and instrument geometry. In particular, the horizontal width of the SO peak is mainly determined by the correlations along the $[-1, 1, 0]$ direction, while the vertical width is dominated by c-axis correlations, elongating the envelope vertically. For the CO peak, the
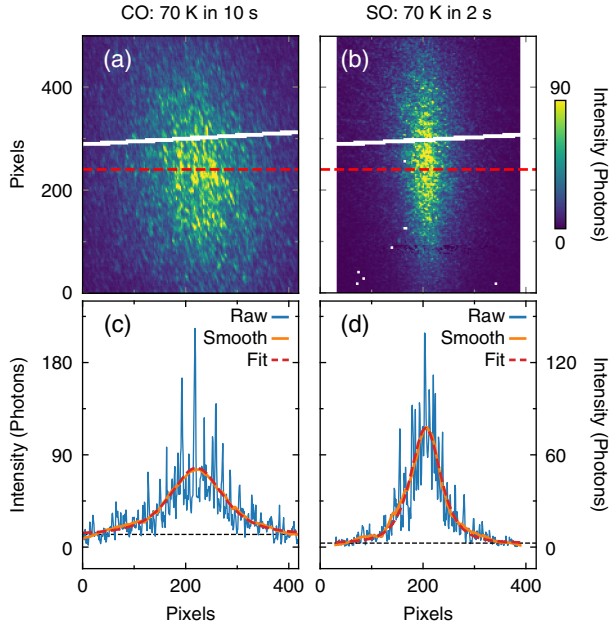
FIG. 2. Speckle patterns of CO and SO. (a),(b) Representative detector images around the CO and SO superlattice peaks measured with a 10 μm pinhole. The white pixels arise from the beamstop or detector errors and are omitted from the data. (c), (d) Line cuts through the horizontal red dashed lines in (a) and (b). The envelope of the peak is estimated by smoothing and fitting processes that are shown as red and orange lines, respectively. The black dashed lines are uniform fluorescent background evaluated from fittings.
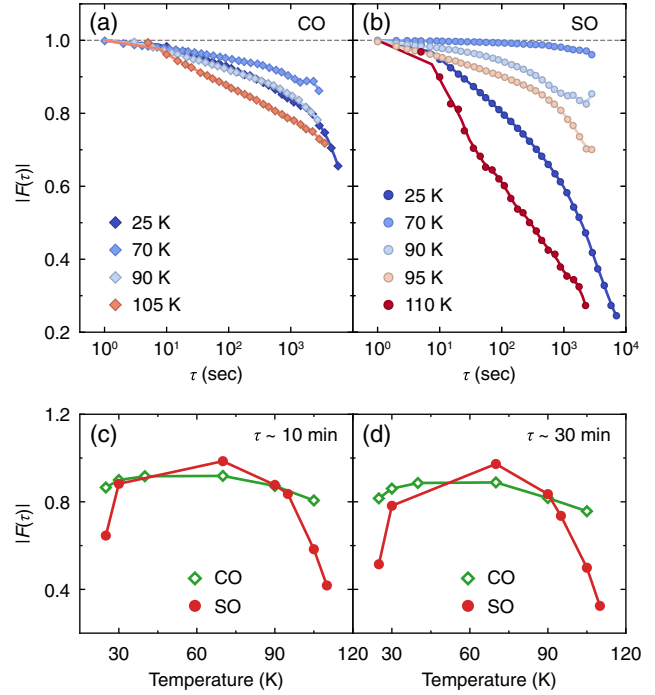

FIG. 3. Temporal stability of CO and SO. (a),(b) Time dependence of the intermediate scattering functions at different temperatures. The solid lines are guides to the eye. (c),(d) The scattering functions after certain time delays.

vertical width has less contribution from c-axis correlations so that the envelope appears more isotropic. Meanwhile, the distribution of the underlying stripe domains is encoded in the positions of the speckles [35], and the shape of the speckles is determined by the Fourier transform of the beam footprint projected onto the detector. The nonzero L component of the CO peak makes the footprint of the beam more anisotropic. To show the speckle modulation more clearly, we present in Figs. 2(c) and 2(d) the line cuts through the red dashed lines in Figs. 2(a) and 2(b). The peak envelope is estimated by two independent methods: smoothing with the Savitzky-Golay filter and fitting with a squared Lorentzian function. The sharp speckle modulation observed here indicates that the fluctuations for CO and SO are slower than the time window of the measurements, which is 1 s at 70 K [39]. Otherwise, the contrast of the interference patterns will be significantly reduced [33].

In order to quantify the fluctuation timescale, we measure the time dependence of the speckle patterns and calculate the normalized one-time correlation function [33]

$$g_2(\tau) = \frac{\langle I(t)I(t+\tau)\rangle}{\langle I(t)\rangle^2} = 1 + \beta|F(\tau)|^2, \quad (1)$$

where I represents the total intensity including background, τ is the lag time, and $\langle\cdots\rangle$ stands for the time and ensemble average. The time-dependent evolution can be extracted from the intermediate scattering function $|F(\tau)|$, which describes the correlation of the speckle patterns separated by a certain time delay. In a statically ordered system, $|F(\tau)|$ will remain unchanged, while speckle dynamics causes it to drop as a function of the time delay. Distinct from $La_{2-x}Ba_xCuO_4$ (LBCO), in which the CO is static over a timescale of at least 2 h [33,34], $|F(\tau)|$ in LSNO decays after several minutes for both CO and SO, indicating charge and spin dynamics (Fig. 3). Moreover, we find that CO and SO are both most stable around 70 K when they have longest correlation lengths, but SO is more stable than CO at 70 K. Although stripes involve a comodulation of both charge and spin [30], we observe that these have different thermal evolution. As the temperature is driven away from 70 K, the temporal stability for SO decreases faster, indicating that SO is less stable against temperature changes. A qualitatively, but not quantitatively, similar trend in SO was reported recently in Ref. [36]. The longer timescales observed here may reflect sample discrimination in strontium and oxygen compositions or improved coherent flux and stability at CSX compared to the Advanced Light Source.

From simple energetic considerations, if an order is less temporally stable and has shorter correlation lengths, one would expect it to be more fragile to thermal disturbance.
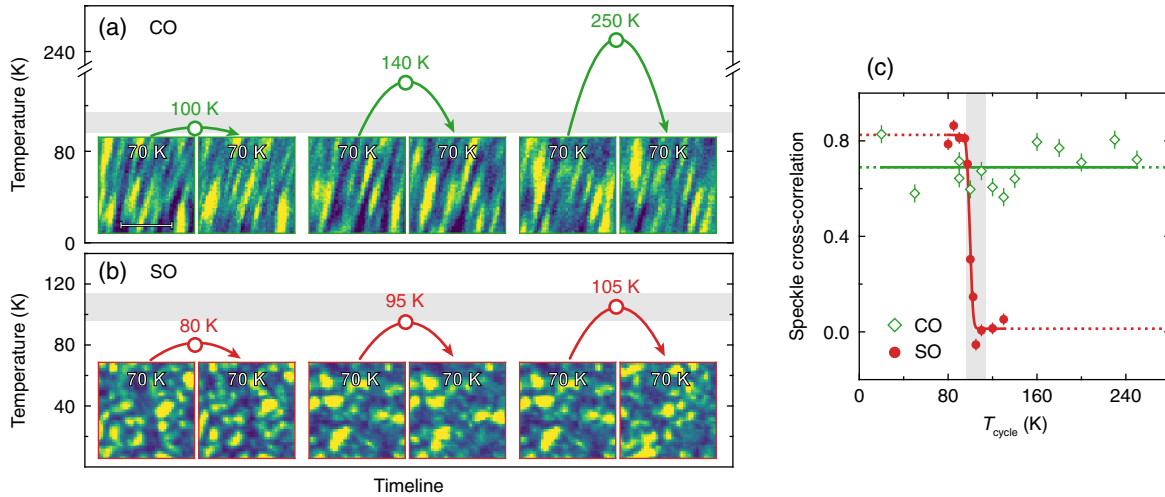
FIG. 4. Domain memory in CO but not SO. (a),(b) Representative speckle images before and after thermal cyclings, which are indicated by the curved arrows. The open circles stand for the cycling temperatures T_{cycle}. For each measurement, we collected images at 70 K, changed the temperature to T_{cycle}, and waited for 10 min. Then the sample was cooled back to 70 K and equilibrated for 30 min before collecting another image. For both the heating and cooling processes, the temperature ramping rate was fixed to 4 K/ min. The white bar in the first speckle image indicates 10^{-3} Å^{-1}. (c) Temperature dependence of the normalized speckle cross-correlation function ξ_{CC}. The solid and dashed lines are guides to the eye. The shaded area indicates the range of CO and SO transition temperatures.

The unexpected robustness of CO against temperature changes indicates that CO is coupled to other degrees of freedom which constrain the CO domains during and after the charge condensation (Fig. 3). Such hypotheses can be examined more deeply in terms of domain-pinning memory effects. Since the speckle positions are primarily determined by the positions of the ordering domains, the comparison of speckle patterns collected at 70 K before and after cycling the sample temperature to T_{cycle} can evaluate whether the domain distributions are reproduced [35]. The usage of a Pt mask further ensures that the illuminated sample volume is fixed throughout the thermal cycling [Fig. 1(b)]. It turns out that the speckle patterns of CO are rather similar with T_{cycle} up to 250 K, well above T_{CO} [Fig. 4(a)]. The SO speckles, however, change their positions once T_{cycle} crosses T_{SO} (~100 K) [Fig. 4(b)]. This effect can be quantified by calculating the normalized cross-correlation function ξ_{CC} which describes the similarity between two speckle patterns [35,39]. ξ_{CC} approaches zero when the two speckle images are different, while two identical images will give ξ_{CC} of one. Correspondingly, we calculate ξ_{CC} for both CO and SO speckle patterns with different T_{cycle} [Fig. 4(c)]. The results again show that CO domain distributions are essentially unchanged after thermal cycling to a temperature far above T_{CO}, while the SO speckle pattern loses reproducibility after the system is driven into the disordered state.

The domain memory effect of CO is caused by coupling to the host lattice. Local potentials arising from structural disorder induced, for example, by Sr doping, structural domain boundaries, or octahedral tilts provide nucleation centers for the CO domains and effectively pin the domains during stripe condensation. Since the average lattice structure of LSNO has translational symmetry over a length scale smaller than CO wavelength, it cannot, itself, pin the CO domains into reproducible locations. In charge-ordered cuprate LBCO, the speckle pattern of CO domains loses memory after the sample is heated across the transition temperature from the low-temperature-orthorhombic (LTO) phase into the high-temperature-tetragonal (HTT) phase [35]. Thus, it is expected that the pinning landscape for CO in LBCO is constrained by twin boundaries created by the LTO structural distortion. In LSNO, the lattice remains in the HTT phase and no long-range LTO distortion is observed [53]. However, short-range stripe-related distortions have been reported to persist up to high temperatures [54]. It is possible that either these distortions or local defects due to Sr-related doping disorder determine the pinning landscape of LSNO in a similar manner.

The pinning effect of CO to the structural disorder also evinces the relevance of EPC in nickelates, which has been illustrated by the discovery of phonon anomalies and nematic behaviors in LSNO [55–58]. It has been argued theoretically that without EPC CO will remain dynamic and not order [32]. For structure-driven CO, phonons soften to zero energy and drag the valence charge along with it to form spatial modulations. Here, however, phonons are softened by a maximum of 20% [56], and charge stripes are formed to reduce Coulomb interactions. EPC helps pin preformed charge stripes according to the lattice symmetry, promoting the static CO. The presence of EPC further couples the CO domains to structural disorder, which strengthens the CO against thermal fluctuations. Consequently, when CO and SO lose correlations

progressively upon heating or cooling away from 70 K, the fluctuations of CO speckles increase more slowly (Fig. 3).

SO behaves in a different way. During the formation of SO, the spins can align either parallel or antiparallel to their quantization axis. This would disrupt the reproducibility of SO speckles after thermal cycling across T_{SO} even if the domain walls are in the same place (Fig. 4). Moreover, the rotational degree of freedom provides an additional fluctuation channel to the ordered spins, facilitating the loss of SO stability when driven away from 70 K (Fig. 3). This is in line with the observation of spin reorientation in LSNO at low temperatures [24,27,38].

The robustness of CO stability and its pinning to the lattice demonstrate that the stripe order in LSNO is charge driven. This directly verifies prior theoretical predictions based on Landau theory of coupled charge and spin order parameters [30] and may reflect that stripe order is charge driven, in general. Our approach will be extendable to other materials and even to other degrees of freedom such as orbital order, bringing a powerful means to disentangle the formation mechanisms of intertwined ground states.

*yshen@bnl.gov
†mdean@bnl.gov

[1] A. V. Chumak, V. I. Vasyuchka, A. A. Serga, and B. Hillebrands, Magnon spintronics, Nat. Phys. **11,** 453 (2015).

[2] E. Fradkin, S. A. Kivelson, and J. M. Tranquada, Theory of intertwined orders in high temperature superconductors, Rev. Mod. Phys. **87,** 457 (2015).

[3] S. Mori, C. H. Chen, and S. W. Cheong, Pairing of charge-ordered stripes in $(La, Ca)MnO_3$, Nature (London) **392,** 473 (1998).

[4] P. A. Lee, N. Nagaosa, and X.-G. Wen, Doping a Mott insulator: Physics of high-temperature superconductivity, Rev. Mod. Phys. **78,** 17 (2006).

[5] H. Ulbrich and M. Braden, Neutron scattering studies on stripe phases in non-cuprate materials, Physica (Amsterdam) **481C,** 31 (2012).

[6] R. Comin and A. Damascelli, Resonant x-ray scattering studies of charge order in cuprates, Annu. Rev. Condens. Matter Phys. **7,** 369 (2016).

[7] J. M. Tranquada, B. J. Sternlieb, J. D. Axe, Y. Nakamura, and S. Uchida, Evidence for stripe correlations of spins and holes in copper oxide superconductors, Nature (London) **375,** 561 (1995).

[8] H. A. Mook, P. Dai, F. Dogan, and R. D. Hunt, One-dimensional nature of the magnetic fluctuations in $YBa_2Cu_3O_{6.6}$, Nature (London) **404,** 729 (2000).

[9] J. E. Hoffman, E. W. Hudson, K. M. Lang, V. Madhavan, H. Eisaki, S. Uchida, and J. C. Davis, A four unit cell periodic pattern of quasi-particle states surrounding vortex cores in $Bi_2Sr_2CaCu_2O_{8+\delta}$, Science **295,** 466 (2002).

[10] J. M. Tranquada, D. J. Buttrey, V. Sachan, and J. E. Lorenzo, Simultaneous Ordering of Holes and Spins in $La_2NiO_{4.125}$, Phys. Rev. Lett. **73,** 1003 (1994).

[11] J. M. Tranquada, D. J. Buttrey, and V. Sachan, Incommensurate stripe order in $La_{2-x}Sr_xNiO_4$ with $x = 0.225$, Phys. Rev. B **54,** 12318 (1996).

[12] D. Li, K. Lee, B. Y. Wang, M. Osada, S. Crossley, H. R. Lee, Y. Cui, Y. Hikita, and H. Y. Hwang, Superconductivity in an infinite-layer nickelate, Nature (London) **572,** 624 (2019).

[13] J. Zhang, Y.-S. Chen, D. Phelan, H. Zheng, M. R. Norman, and J. F. Mitchell, Stacked charge stripes in the quasi-2D trilayer nickelate $La_4Ni_3O_8$, Proc. Natl. Acad. Sci. U.S.A. **113,** 8945 (2016).

[14] J. Zhang, A. S. Botana, J. W. Freeland, D. Phelan, H. Zheng, V. Pardo, M. R. Norman, and J. F. Mitchell, Large orbital polarization in a metallic square-planar nickelate, Nat. Phys. **13,** 864 (2017).

[15] J. Zhang, D. M. Pajerowski, A. S. Botana, H. Zheng, L. Harriger, J. Rodriguez-Rivera, J. P. C. Ruff, N. J. Schreiber, B. Wang, Y.-S. Chen, W. C. Chen, M. R. Norman, S. Rosenkranz, J. F. Mitchell, and D. Phelan, Spin Stripe Order in a Square Planar Trilayer Nickelate, Phys. Rev. Lett. **122,** 247201 (2019).

[16] J. Q. Lin et al., Strong Superexchange in a $d^{9-\delta}$ Nickelate Revealed by Resonant Inelastic X-Ray Scattering, Phys. Rev. Lett. **126,** 087001 (2021).

[17] V. J. Emery, S. A. Kivelson, and O. Zachar, Spin-gap proximity effect mechanism of high-temperature superconductivity, Phys. Rev. B **56,** 6120 (1997).

[18] S. A. Kivelson, E. Fradkin, and V. J. Emery, Electronic liquid-crystal phases of a doped mott insulator, Nature (London) **393,** 550 (1998).

[19] D. F. Agterberg, J. C. Séamus Davis, S. D. Edkins, E. Fradkin, D. J. Van Harlingen, S. A. Kivelson, P. A. Lee, L. Radzihovsky, J. M. Tranquada, and Y. Wang, The physics of pair-density waves: Cuprate superconductors and beyond, Annu. Rev. Condens. Matter Phys. **11,** 231 (2020).

[20] C. H. Chen, S. W. Cheong, and A. S. Cooper, Charge Modulations in $La_{2-x}Sr_xNiO_{4+y}$: Ordering of Polarons, Phys. Rev. Lett. **71,** 2461 (1993).

[21] S. W. Cheong, H. Y. Hwang, C. H. Chen, B. Batlogg, L. W. Rupp, and S. A. Carter, Charge-ordered states in $(La, Sr)_2NiO_4$ for hole concentrations $n_h = 1/3$ and $1/2$, Phys. Rev. B **49,** 7088 (1994).

[22] S. H. Lee and S. W. Cheong, Melting of Quasi-Two-Dimensional Charge Stripes in $La_{5/3}Sr_{1/3}NiO_4$, Phys. Rev. Lett. **79**, 2514 (1997).

[23] H. Yoshizawa, T. Kakeshita, R. Kajimoto, T. Tanabe, T. Katsufuji, and Y. Tokura, Stripe order at low temperatures in $La_{2-x}Sr_xNiO_4$ with $0.289 \lesssim x \lesssim 0.5$, Phys. Rev. B **61**, R854 (2000).

[24] S. H. Lee, S. W. Cheong, K. Yamada, and C. F. Majkrzak, Charge and canted spin order in $La_{2-x}Sr_xNiO_4$ ($x = 0.275$ and 1/3), Phys. Rev. B **63**, 060405(R) (2001).

[25] R. Kajimoto, T. Kakeshita, H. Yoshizawa, T. Tanabe, T. Katsufuji, and Y. Tokura, Hole concentration dependence of the ordering process of the stripe order in $La_{2-x}Sr_xNiO_4$, Phys. Rev. B **64**, 144432 (2001).

[26] M. E. Ghazi, P. D. Spencer, S. B. Wilkins, P. D. Hatton, D. Mannix, D. Prabhakaran, A. T. Boothroyd, and S. W. Cheong, Incommensurate charge stripe ordering in $La_{2-x}Sr_xNiO_4$ for $x = (0.33, 0.30, 0.275)$, Phys. Rev. B **70**, 144507 (2004).

[27] P. G. Freeman, A. T. Boothroyd, D. Prabhakaran, M. Enderle, and C. Niedermayer, Stripe order and magnetic transitions in $La_{2-x}Sr_xNiO_4$, Phys. Rev. B **70**, 024413 (2004).

[28] M. Raczkowski, R. Frésard, and A. M. Oleś, Microscopic origin of diagonal stripe phases in doped nickelates, Phys. Rev. B **73**, 094429 (2006).

[29] P. Wochner, J. M. Tranquada, D. J. Buttrey, and V. Sachan, Neutron-diffraction study of stripe order in $La_2NiO_{4+\delta}$ with $\delta = 2/15$, Phys. Rev. B **57**, 1066 (1998).

[30] O. Zachar, S. A. Kivelson, and V. J. Emery, Landau theory of stripe phases in cuprates and nickelates, Phys. Rev. B **57**, 1422 (1998).

[31] J. Zaanen and P. B. Littlewood, Freezing electronic correlations by polaronic instabilities in doped La_2NiO_4, Phys. Rev. B **50**, 7222 (1994).

[32] T. Hotta and E. Dagotto, Orbital Ordering, New Phases, and Stripe Formation in Doped Layered Nickelates, Phys. Rev. Lett. **92**, 227201 (2004).

[33] X. M. Chen, V. Thampy, C. Mazzoli, A. M. Barbour, H. Miao, G. D. Gu, Y. Cao, J. M. Tranquada, M. P. M. Dean, and S. B. Wilkins, Remarkable Stability of Charge Density Wave Order in $La_{1.875}Ba_{0.125}CuO_4$, Phys. Rev. Lett. **117**, 167001 (2016).

[34] V. Thampy, X. M. Chen, Y. Cao, C. Mazzoli, A. M. Barbour, W. Hu, H. Miao, G. Fabbris, R. D. Zhong, G. D. Gu, J. M. Tranquada, I. K. Robinson, S. B. Wilkins, and M. P. M. Dean, Static charge-density-wave order in the superconducting state of $La_{2-x}Ba_xCuO_4$, Phys. Rev. B **95**, 241111(R) (2017).

[35] X. M. Chen, C. Mazzoli, Y. Cao, V. Thampy, A. M. Barbour, W. Hu, M. Lu, T. A. Assefa, H. Miao, G. Fabbris, G. D. Gu, J. M. Tranquada, M. P. M. Dean, S. B. Wilkins, and I. K. Robinson, Charge density wave memory in a cuprate superconductor, Nat. Commun. **10**, 1435 (2019).

[36] A. Ricci, N. Poccia, G. Campi, S. Mishra, L. Müller, B. Joseph, B. Shi, A. Zozulya, M. Buchholz, C. Trabant, J. C. T. Lee, J. Viefhaus, J. B. Goedkoop, A. A. Nugroho, M. Braden, S. Roy, M. Sprung, and C. Schüßler-Langeheine, Intrinsic spatial and temporal destabilization of incommensurate stripes at low temperatures, arXiv:1912.07306.

[37] D. Prabhakaran, P. Isla, and A. T. Boothroyd, Growth of large $La_{2-x}Sr_xNiO_{4+\delta}$ single crystals by the floating-zone technique, J. Cryst. Growth **237–239**, 815 (2002).

[38] P. G. Freeman, A. T. Boothroyd, D. Prabhakaran, and J. Lorenzana, Magnetization of $La_{2-x}Sr_xNiO_{4+\delta}$ ($0 \ll x \ll 0.5$): Spin-glass and memory effects, Phys. Rev. B **73**, 014434 (2006).

[39] See Supplemental Material at http://link.aps.org/supplemental/10.1103/PhysRevLett.126.177601 for details of the x-ray measurements, sample preparation and the wave vectors of charge and spin order peaks.

[40] National Syncrotron light Source II Website, https://www.bnl.gov/ps/accelerator/, accessed: 2020-12-02.

[41] C. Schüssler-Langeheine, J. Schlappa, A. Tanaka, Z. Hu, C. F. Chang, E. Schierle, M. Benomar, H. Ott, E. Weschke, G. Kaindl, O. Friedt, G. A. Sawatzky, H.-J. Lin, C. T. Chen, M. Braden, and L. H. Tjeng, Spectroscopy of Stripe Order in $La_{1.8}Sr_{0.2}NiO_4$ Using Resonant Soft X-Ray Diffraction, Phys. Rev. Lett. **95**, 156402 (2005).

[42] J. Fink, E. Schierle, E. Weschke, and J Geck, Resonant elastic soft x-ray scattering, Rep. Prog. Phys. **76**, 056502 (2013).

[43] R. Kukreja, N. Hua, J. Ruby, A. Barbour, W. Hu, C. Mazzoli, S. Wilkins, E. E. Fullerton, and O. G. Shpyrko, Orbital Domain Dynamics in Magnetite below the Verwey Transition, Phys. Rev. Lett. **121**, 177601 (2018).

[44] $\xi = a/\sqrt{2}\Delta H$ where ΔH is half width at half maximum change in ΔH for a $[H, H, 0]$ scan.

[45] P. D. Hatton, M. E. Ghazi, S. B. Wilkins, P. D. Spencer, D. Mannix, T. d'Almeida, P. Prabhakaran, A. Boothroyd, and S. W. Cheong, X-ray scattering studies of charge stripes in $La_{2-x}Sr_xNiO_4$ ($x = 0.20$–0.33), Physica (Amsterdam) **318B**, 289 (2002).

[46] J. Schlappa, C. F. Chang, E. Schierle, A. Tanaka, R. Feyerherm, Z. Hu, H. Ott, O. Friedt, E. Dudzik, H. H. Hung, M. Benomar, M. Braden, L. H. Tjeng, and C. Schüßler-Langeheine, Static and fluctuating stripe order observed by resonant soft x-ray diffraction in $La_{1.8}Sr_{0.2}NiO_4$, arXiv:0903.0994.

[47] V. Sachan, D. J. Buttrey, J. M. Tranquada, J. E. Lorenzo, and G. Shirane, Charge and spin ordering in $La_{2-x}Sr_xNiO_{4.00}$ with $x = 0.135$ and 0.20, Phys. Rev. B **51**, 12742 (1995).

[48] K. Ishizaka, T. Arima, Y. Murakami, R. Kajimoto, H. Yoshizawa, N. Nagaosa, and Y. Tokura, Commensurate-Incommensurate Crossover of Charge Stripe in $La_{2-x}Sr_xNiO_4$ ($x \sim 1/3$), Phys. Rev. Lett. **92**, 196404 (2004).

[49] H. Miao, R. Fumagalli, M. Rossi, J. Lorenzana, G. Seibold, F. Yakhou-Harris, K. Kummer, N. B. Brookes, G. D. Gu, L. Braicovich, G. Ghiringhelli, and M. P. M. Dean, Formation of Incommensurate Charge Density Waves in Cuprates, Phys. Rev. X **9**, 031042 (2019).

[50] S. Brauer, G. B. Stephenson, M. Sutton, R. Brüning, E. Dufresne, S. G. J. Mochrie, G. Grübel, J. Als-Nielsen, and D. L. Abernathy, X-Ray Intensity Fluctuation Spectroscopy Observations of Critical Dynamics in Fe_3Al, Phys. Rev. Lett. **74**, 2010 (1995).

[51] O. Shpyrko, X-ray photon correlation spectroscopy, J. Synchrotron Radiat. **21**, 1057 (2014).

[52] S. Lee, J. Jiang, G. Fabbris, A. S. Disa, M. P. M. Dean, S. Ismail-Beigi, F. J. Walker, C. Mazzoli, and C. H. Ahn,

Dimensionality-driven antiferromagnetic dynamics in nick-elate heterostructures (to be published).

[53] M. Hücker, K. Chung, M. Chand, T. Vogt, J. M. Tranquada, and D. J. Buttrey, Oxygen and strontium codoping of La$_2$NiO$_4$: Room-temperature phase diagrams, Phys. Rev. B **70**, 064105 (2004).

[54] A. M. Milinda Abeykoon, E. S. Božin, W.-G. Yin, G. Gu, J. P. Hill, J. M. Tranquada, and S. J. L. Billinge, Evidence for Short-Range-Ordered Charge Stripes far above the Charge-Ordering Transition in La$_{1.67}$Sr$_{0.33}$NiO$_4$, Phys. Rev. Lett. **111**, 096404 (2013).

[55] Yu. G. Pashkevich, V. A. Blinkin, V. P. Gnezdilov, V. V. Tsapenko, V. V. Eremenko, P. Lemmens, M. Fischer, M. Grove, G. Güntherodt, L. Degiorgi, P. Wachter, J. M. Tranquada, and D. J. Buttrey, Stripe Conductivity in La$_{1.775}$Sr$_{0.225}$NiO$_4$, Phys. Rev. Lett. **84**, 3919 (2000).

[56] J. M. Tranquada, K. Nakajima, M. Braden, L. Pintschovius, and R. J. McQueeney, Bond-Stretching-Phonon Anomalies in Stripe-Ordered La$_{1.69}$Sr$_{0.31}$NiO$_4$, Phys. Rev. Lett. **88**, 075505 (2002).

[57] A. M. Merritt, A. D. Christianson, A. Banerjee, G. D. Gu, A. S. Mishchenko, and D. Reznik, Giant electron–phonon coupling of the breathing plane oxygen phonons in the dynamic stripe phase of La$_{1.67}$Sr$_{0.33}$NiO$_4$, Sci. Rep. **10**, 11426 (2020).

[58] R. Zhong, B. L. Winn, G. Gu, D. Reznik, and J. M. Tranquada, Evidence for a Nematic Phase in La$_{1.75}$Sr$_{0.25}$NiO$_4$, Phys. Rev. Lett. **118**, 177601 (2017).